

# Climate extreme event attribution using multivariate peaks-over-thresholds modeling and counterfactual theory

Anna Kiriliouk\*

Faculté des sciences économiques,  
sociales et de gestion  
Universit de Namur, Belgium.

Philippe Naveau

Laboratoire des Sciences du Climat  
et de l'Environnement (LSCE)  
CNRS, Gif-sur-Yvette, France

## Abstract

Numerical climate models are complex and combine a large number of physical processes. They are key tools to quantify the relative contribution of potential anthropogenic causes (e.g., the current increase in greenhouse gases) on high impact atmospheric variables like heavy rainfall. These so-called climate extreme event attribution problems are particularly challenging in a multivariate context, that is, when the atmospheric variables are measured on a possibly high-dimensional grid.

In this paper, we leverage two statistical theories to assess causality in the context of multivariate extreme event attribution. As we consider an event to be extreme when at least one of the components of the vector of interest is large, extreme-value theory justifies, in an asymptotical sense, a multivariate generalized Pareto distribution to model joint extremes. Under this class of distributions, we derive and study probabilities of necessary and sufficient causation as defined by the counterfactual theory of Pearl. To increase causal evidence, we propose a dimension reduction strategy based on the optimal linear projection that maximizes such causation probabilities. Our approach is tested on simulated examples and applied to weekly winter maxima precipitation outputs of the French CNRM from the recent CMIP6 experiment.

*Keywords:* multivariate generalized Pareto distribution, necessary and sufficient causation, heavy rainfall and climate change

---

\*Part of this work was supported by the French national program FRAISE-LEFE/INSU, MELODY-ANR, Eupheme, FUSIMET (PEPS I3A) and the DAMOCLES-COST-ACTION on compound events.

# 1 Introduction

Quantifying human influence on climate change and identifying potential causes of climate extremes is often referred to as extreme event attribution (EEA), which falls within the research field of detection and attribution (D&A) (see, e.g. the report of National Academies of Sciences, Engineering and Medicine 2016, Chen et al. 2018). In such studies, the main inferential objective is estimation of extreme quantiles (return levels), well-used in finance, hydrology and other fields of risk analysis (e.g. Embrechts et al. 1997). In EEA, such small probabilities and their associated return levels are computed under two scenarios that differ according to the causal link of interest, often increases in greenhouse gases (GHG) concentrations (see, e.g. Angélil et al. 2017, Stott et al. 2016, Fischer & Knutti 2015). Typically, such an approach compares probabilities under a factual scenario of conditions that occurred around the time of the event against probabilities under a counterfactual scenario in which anthropogenic emissions never occurred. Under this set-up, one can compare the probability of an extreme event in the factual world, denoted  $p_1$ , to the probability of an extreme event  $p_0$  in a counterfactual world, i.e., a world that might have been if no anthropogenic forcing would have existed. The definition of the so-called extreme event is by itself a non-trivial task and depends on the application at hand. A common choice is to take some climatic index exceeding a high threshold. In their seminal paper, Stott et al. (2004) studied mean June-August temperatures in Europe in order to quantify by how much human activities may have increased the risk of European heatwaves. In this example, a one dimensional sample mean, say  $Y$ , summarized a complex random field that varied in time and space. The set  $\{Y > v\}$  where  $v = 1.6$  Kelvin was chosen to resemble the 2003 mean European summer anomaly temperatures. The probabilities  $p_0$  and  $p_1$  were then inferred from numerical counterfactual and factual runs respectively, using non-parametric

inference techniques (for bootstrap counting methods in EEA, see Paciorek et al. 2018) and univariate extreme-value theory (EVT); for an EVT introduction, see, e.g. Coles (2001). For trend detection problems in D&A, there exists a variety of EVT models, see e.g. the pioneering work of Kharin & Zwiers (2005) and Kharin et al. (2007).

In other environmental research areas, complex multivariate EVT models are commonly used (see, e.g. Davison & Huser 2015, Cooley et al. 2017, de Fondeville & Davison 2019, 2018, Engelke et al. 2018, Reich et al. 2013, Engelke et al. 2018, Shaby & Reich 2012). Bayesian hierarchical modeling (see, e.g. Hammerling et al. 2017, Katzfuss et al. 2017) also offers a flexible way to insert different layers of complexity present in climate D&A problems (internal natural variability, numerical model uncertainty, observational errors, sampling uncertainty in space and time, etc.). Despite these advances, the EEA domain remains a fairly untouched territory in terms of multivariate EVT. Even recent applied papers like Kew et al. (2019), Luu et al. (2018), Otto et al. (2018) and King (2017) are based on univariate EVT only.

Our first objective is to investigate how multivariate EVT could be used for event attribution. As extreme events in D&A are mostly expressed in terms of threshold exceedances, like  $\{Y > v\}$  in Stott et al. (2004), this naturally leads to the question of how to integrate the multivariate generalized Pareto distribution (GPD) introduced by Tajvidi (1996) into the EEA framework. This distribution has been tailored to represent extremal behaviors when at least one of the components of the vector of interest is large. The probabilistic properties of the multivariate GPD have been well studied by, among others, Beirlant et al. (2004), Rootzén & Tajvidi (2006), Falk & Guillou (2008), Ferreira & de Haan (2014), Rootzén et al. (2018b) and Rootzén et al. (2018a), while statistical modeling is more recent (Huser et al. 2016, Kiriliouk et al. 2019).

In most univariate EEA studies (see Stott et al. 2016, and references therein), two

types of probability ratios are considered: the Risk Ratio  $\frac{p_1}{p_0}$  and the so-called Fraction of Attributable Risk (FAR), defined by

$$\text{FAR} = 1 - \frac{p_0}{p_1},$$

where  $p_0 = P(X > v)$  corresponds to probability of exceeding the threshold  $v$  in the counterfactual world, while  $p_1$  represents the same quantity in the factual world. Using the counterfactual theory of Pearl (2000), the FAR corresponds to the probability of necessary causation, i.e., anthropogenic forcings are necessary for the extreme event to occur, but might not be sufficient. Within the Gaussian set-up, Hannart et al. (2016) and Hannart & Naveau (2018) highlighted the link between causality theory and event attribution studies. The second objective of our work is to explain how Pearl's counterfactual theory can be applied within a multivariate GPD framework, and to identify conditions that increase the level of causality, a fundamental feature in any EEA analysis.

The rest of the paper is structured as follows. Section 2 summarizes the relevant background of both multivariate GPDs and climate event attribution. Section 3 discusses the behaviour of univariate probabilities of causation as a function of the threshold  $v$ . In Section 4, we make the link between multivariate GPDs and causality by maximizing necessary causation for any linear projection and we discuss the inference strategy. Finally, in Section 5, the proposed methods are applied to weekly winter maxima of precipitation outputs from the French CNRM model that are part of the recent CMIP6 experiment. Technical details are deferred to the appendices.

## 2 Background

### 2.1 The multivariate generalized Pareto distribution

The basic building block to construct standardized multivariate GPD random vectors (Rootzén & Tajvidi 2006, Rootzén et al. 2018b) is the stochastic representation

$$\mathbf{Z}^* \stackrel{d}{=} E + \mathbf{T} - \max_{1 \leq j \leq d} T_j, \quad (2.1)$$

where  $E$  corresponds to a univariate exponential random variable with unit mean, and  $\mathbf{T} = (T_1, \dots, T_d)^T$  represents any  $d$ -dimensional random vector independent of  $E$ . One can easily check that each positive conditional margin has a unit exponential survival function,

$$\mathbb{P}[Z_j^* > z \mid Z_j^* > 0] = \exp(-z), \quad \text{for any } z > 0 \text{ and } j \in \{1, \dots, d\}.$$

Model (2.1) can be generalized by setting, for  $\boldsymbol{\sigma} > \mathbf{0}$  and  $\boldsymbol{\gamma} \in \mathbb{R}^d$ ,

$$\mathbf{Z} \stackrel{d}{=} \frac{\boldsymbol{\sigma}}{\boldsymbol{\gamma}} (\exp(\boldsymbol{\gamma} \mathbf{Z}^*) - 1), \quad (2.2)$$

where operations like  $\frac{\boldsymbol{\sigma}}{\boldsymbol{\gamma}}$  have to be understood componentwise. We then denote  $\mathbf{Z} \sim \text{MGPD}(\mathbf{T}, \boldsymbol{\sigma}, \boldsymbol{\gamma})$ . Equation (2.2) implies

$$\mathbb{P}[Z_j > z \mid Z_j > 0] = \overline{H}(z; \sigma_j, \gamma_j), \quad \text{for any } z > 0 \text{ and } j \in \{1, \dots, d\},$$

where  $\overline{H}(z; \sigma, \gamma) = (1 + \gamma z / \sigma)_+^{-1/\gamma}$  denotes the survival function of the univariate GPD with scale parameter  $\sigma > 0$  and shape parameter  $\gamma \in \mathbb{R}$ . Hence, the conditional margins  $[Z_j \mid Z_j > 0]$  follow univariate GPDs<sup>1</sup>.

Theoretically, the random vector  $\mathbf{Z}$  defined by (2.1) and (2.2) can be viewed as the limiting solution of any linearly rescaled multivariate vector given that at least one component

---

<sup>1</sup>although the random variables  $Z_1, \dots, Z_d$  may not follow GPDs themselves.

is large (Rootzén & Tajvidi 2006, Rootzén et al. 2018b). This asymptotic result can be interpreted as a multivariate version of the Pickands–Balkema–de Haan theorem (Pickands 1975, Balkema & de Haan 1974).

Let  $\mathbf{X}$  denote a random vector in  $\mathbb{R}^d$ , representing a  $d$ -variate observation, and let  $\mathbf{u} \in \mathbb{R}^d$  denote a high threshold. When  $d = 1$ , univariate peaks-over-thresholds approaches (Davison & Smith 1990) consist of fitting  $[X - u \mid X > u]$  to a univariate GPD. Similarly, the multivariate GPD approximates the tail behavior of  $[\mathbf{X} - \mathbf{u} \mid \mathbf{X} \not\leq \mathbf{u}]$ , where  $\mathbf{X} \not\leq \mathbf{u}$  means that at least one component of  $\mathbf{X}$  exceeds the corresponding component of  $\mathbf{u}$ . By construction, multivariate GPD vectors exhibit *asymptotic dependence*, i.e.,  $[\mathbf{X} - \mathbf{u} \mid \mathbf{X} \not\leq \mathbf{u}]$  is well-approximated by a member of the class of multivariate GPDs if  $\mathbf{X}$  puts no mass on lower-dimensional subspaces.

The random “generator”  $\mathbf{T}$  in (2.1) drives the extremal dependence of  $\mathbf{Z}$ , often summarized by the *tail dependence coefficient*  $\chi \in [0, 1]$ . If  $F_1, F_2$  denote the unconditional marginal distribution functions of  $Z_1, Z_2$ , then  $\chi$  measures the probability of  $F_1(Z_1)$  being large given that  $F_2(Z_2)$  is large as the threshold increases,

$$\chi = \lim_{q \uparrow 1} \mathbb{P}[F_1(Z_1) > q \mid F_2(Z_2) > q] = \mathbb{E} \left[ \min \left( \frac{e^{T_1 - \max(T_1, T_2)}}{\mathbb{E}[e^{T_1 - \max(T_1, T_2)}]}, \frac{e^{T_2 - \max(T_1, T_2)}}{\mathbb{E}[e^{T_2 - \max(T_1, T_2)}]} \right) \right].$$

A large value of  $\chi$  corresponds to strong extremal dependence between  $Z_1$  and  $Z_2$ , whereas  $\chi = 0$  corresponds to tail independence. For more details on  $\chi$  in the context of multivariate GPDs, see the supplementary material in Kiriliouk et al. (2019). As an example, Figure 1 displays 500 bivariate random draws from a multivariate GPD model where  $\mathbf{T}$  is zero-mean bivariate Gaussian with unit covariance matrix  $I_2$ , corresponding to  $\chi = 0.6$ .

To make the link with the probabilities  $p_0$  and  $p_1$  used for EEA, we need a tool to project the information contained in a possibility complex multivariate GPD structure into a single valued summary. The following proposition provides this key tool.

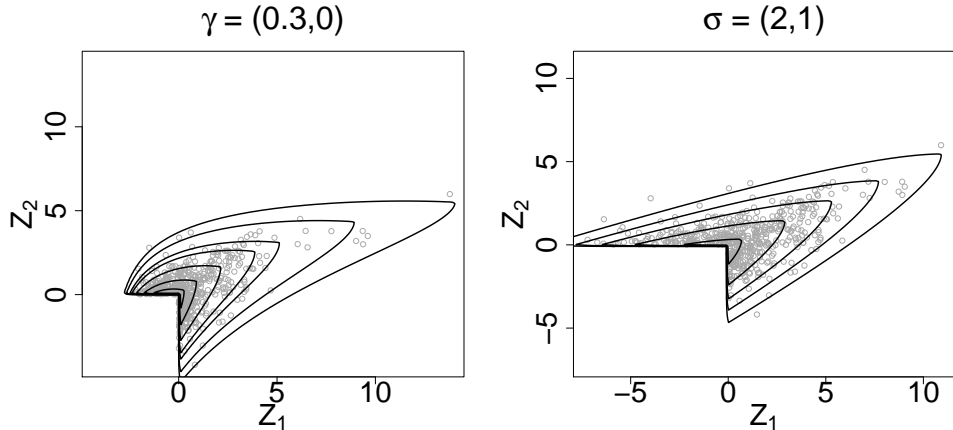


Figure 1: Scatterplots and density contours from 500 bivariate GPD random draws using (2.1) and (2.2) with parameters  $\gamma = (0.3, 0)$ ,  $\sigma = (1, 1)$  for the left panel and  $\gamma = (0, 0)$ ,  $\sigma = (2, 1)$  for the right panel. The generator  $\mathbf{T}$  is zero-mean bivariate Gaussian with unit covariance matrix  $I_2$ .

**Proposition 2.1** (Linear-projection, Rootzén et al. (2018b)). *If  $\mathbf{Z} \sim \text{MGPD}(\mathbf{T}, \sigma, \gamma)$  with  $\gamma = \gamma \mathbf{1}_d$ , then for any non-negative weights  $\mathbf{w} = (w_1, \dots, w_d)^T$  such that  $\mathbb{P}[\mathbf{w}^T \mathbf{Z} > 0] > 0$ , the linear projection of  $\mathbf{Z}$ , conditioned on being positive, follows a univariate GPD, i.e.,*

$$[\mathbf{w}^T \mathbf{Z} \mid \mathbf{w}^T \mathbf{Z} > 0] \sim \text{GPD}(\mathbf{w}^T \sigma, \gamma).$$

## 2.2 Climate event attribution and counterfactual theory

The question of attribution in EEA is rooted in causality assessment, so that connections between the probabilities  $p_0$  and  $p_1$  and some type of causality are called for. To explain the link between some event  $E$  (e.g. the 2003 European heatwave) and its potential cause  $C$  (e.g. the increase of GHG emissions), Pearl (2000) makes the distinction between three

forms of causality. These types of causality can be expressed in a probabilistic manner as

1. probability of necessary causation (PN):  $C$  is required for  $E$  but other factors might be required as well;
2. probability of sufficient causation (PS):  $C$  always triggers  $E$  but  $E$  might occur without  $C$ ;
3. probability of necessary and sufficient causation (PNS): both of the above hold.

In most applications, these probabilities are difficult to estimate. In the special case of climate EEA where one assumes that both factual and counterfactual worlds are available from numerical experiments, Hannart et al. (2016) exploited the fact that  $E$  is monotonous with respect to the external forcings (increase in GHGs likely leads to a warmer climate) and all forcings are exogenous (fossil energy, volcanic forcings are not part of the climate system). This simplifies the expressions of PN, PS and PNS that become

$$\text{PN} = \max \left( 1 - \frac{p_0}{p_1}, 0 \right), \quad \text{PS} = \max \left( 1 - \frac{1 - p_1}{1 - p_0}, 0 \right), \quad \text{PNS} = \max (p_1 - p_0, 0), \quad (2.3)$$

where  $p_0 = \mathbb{P}[E \mid \bar{C}]$  is the probability of  $E$  in the counterfactual world and  $p_1 = \mathbb{P}[E \mid C]$  is the probability of  $E$  in the factual world. If  $p_0 < p_1$ , then PN coincides with the FAR used by Stott et al. (2004). In the remainder of this paper, we will use the notation PN (instead of FAR) to highlight its causal interpretation. By construction, one has  $\text{PNS} \leq \min(\text{PN}, \text{PS})$  and hence it is worth noticing that a low PNS does not imply the absence of a causal relationship.

One important objective of this paper is to combine multivariate EVT and causality theory. This leads to the question of how to reduce the dimension of a multivariate GPD vector, while ensuring that the projected data contains the most information in terms

of causality for extremes. In a multivariate Gaussian set-up, Hannart & Naveau (2018) proposed to maximize PNS by taking the linear combination that will contrast the factual and counterfactual worlds the most. Their solution was similar to linear discriminant analysis. Before dealing with the multivariate GPD case, one can learn a lot from studying  $p_0$ ,  $p_1$ , PN, PS and PNS in the univariate case.

### 3 Causation probabilities for univariate extremes

To understand how PN, PS and PNS behave for univariate extremes, we take  $p_0(v) = \mathbb{P}[X^{(0)} > v]$  and  $p_1(v) = \mathbb{P}[X^{(1)} > v]$  when  $X^{(0)}$  and  $X^{(1)}$  are either Gaussian or GPD random variables. The left panel of Figure 2 shows the case where the counterfactual world corresponds to a standardized Gaussian variable,  $X^{(0)} \sim N(0, 1)$ , and the factual world is one Kelvin warmer with a higher variability,  $X^{(1)} \sim N(1, 1.5)$ . This artificial design mimics the typical behaviour of mean temperature anomalies. Two features can be highlighted from this example: PN goes to one as  $v$  increases, and the maximum of PNS is around 0.35. In other words, the probability of necessary causation becomes certain for extremes (large  $v$ ), and the probability of necessary and sufficient causation can be reasonably high in the Gaussian case.

To contrast these remarks with other types of tail behaviors, the middle panel of Figure 2 displays a GPD case with equal shape parameter  $\gamma = 0.2$  in the counterfactual and factual worlds, but different scale parameters,  $\sigma^{(0)} = 1$  and  $\sigma^{(1)} = 1.5$ . One can see that, as  $v$  increases, PN converges to a constant around  $0.7 < 1$ , and PNS remains small for any value of  $v$ . Hence, causal evidencing is much more difficult than in the Gaussian set-up, where a rare event in the factual world ( $p_1$  small) would be nearly impossible in the counterfactual world ( $p_0$  almost zero). In contrast, even a very rare event in the

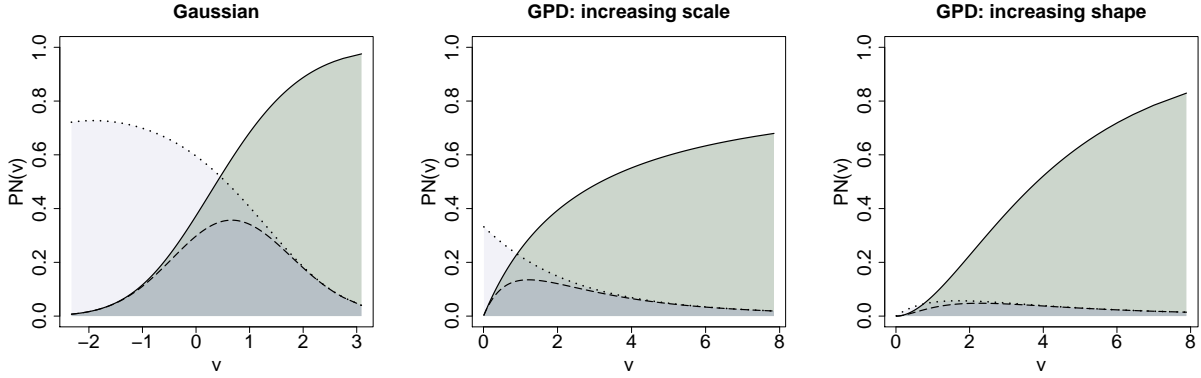


Figure 2: Probabilities of necessary causation (PN, solid line), sufficient causation (PS, dotted line) and sufficient and necessary causation (PNS, dashed line) as functions of  $v$ . The left panel corresponds to a Gaussian set-up:  $N(0, 1)$  for the counterfactual world and  $N(1, 1.5)$  for the factual one. The middle and right panels correspond to a GPD set-up:  $GPD(1, 0.2)$  for the counterfactual world,  $GPD(1.5, 0.2)$  for the factual one (middle) and  $GPD(1, 0.1)$  for the counterfactual world,  $GPD(1, 0.3)$  for the factual one (right).

factual world will not be impossible in a GPD counterfactual world. Concerning PNS, it is small in the second panel and this phenomenon is even more pronounced when the shape parameter changes between the two worlds; see the right panel where  $\gamma^{(0)} = 0.1$ ,  $\gamma^{(1)} = 0.3$ , and  $\sigma^{(0)} = \sigma^{(1)} = 1$ . As PNS is always almost near zero, there is no reason to maximize it. Instead, maximizing causality will correspond to maximizing PN in the remainder of this work.

In practice,  $X^{(0)}$  and  $X^{(1)}$  do not follow GPDs. Using a classical peaks-over-thresholds approach, we can condition on some high threshold  $u^{(i)}$  and approximate the probabilities

$p_i(v) = \mathbb{P}[X^{(i)} > v]$  for  $v > u^{(i)}$  by

$$p_i(v) \approx \mathbb{P}[X^{(i)} > u^{(i)}] \bar{H}(v - u^{(i)}; \sigma^{(i)}, \gamma^{(i)}), \quad \text{for } i \in \{0, 1\}. \quad (3.1)$$

We can now formalize the tail behaviour observed in Figure 2. Whenever the limit of  $\text{PN}(v)$  for large  $v$  is finite<sup>2</sup>, it has to be equal to

$$\begin{cases} \mathbb{1}\{\gamma^{(0)} < \gamma^{(1)}\} & \text{if } \gamma^{(1)} \neq \gamma^{(0)}, \\ 1 - \frac{p_0(u^{(0)})}{p_1(u^{(1)})} \left(\frac{\sigma^{(0)}}{\sigma^{(1)}}\right)^{1/\gamma} & \text{if } \gamma^{(1)} = \gamma^{(0)} =: \gamma, \gamma \neq 0, \\ \mathbb{1}\{\sigma^{(0)} < \sigma^{(1)}\} & \text{if } \gamma^{(1)} = \gamma^{(0)} = 0. \end{cases} \quad (3.2)$$

where  $\mathbb{1}(A)$  represents the indicator function, equal to one if  $A$  is true and zero otherwise.

The left panel of Figure 3 shows how three different GPD shape parameters,  $\gamma = -0.4$ ,  $\gamma = -0.4$  and  $\gamma = -0.4$  (dashed, solid and dotted lines respectively) influence the increase of the PN with respect to the threshold  $v$ . The right panel of Figure 3 points out possible atypical behaviors of the PN, highlighting that  $\text{PN}(v)$  is not always increasing as  $v$  increases. Here, the solid line corresponds to a counterfactual world with  $(\gamma^{(0)}, \sigma^{(0)}) = (0, 2)$  compared to a factual world with  $(\gamma^{(1)}, \sigma^{(1)}) = (0.4, 1)$ , while the dotted line represents the converse change: from  $(\gamma^{(0)}, \sigma^{(0)}) = (0.4, 1)$  to  $(\gamma^{(1)}, \sigma^{(1)}) = (0, 2)$ .

## 4 Necessary causation in a multivariate set-up

### 4.1 The multivariate GPD and necessary causation

Let  $\mathbf{X}$  be any  $d$ -dimensional random vector such that  $[\mathbf{X} - \mathbf{u} \mid \mathbf{X} \not\leq \mathbf{u}] \approx \mathbf{Z}$  for some high threshold  $\mathbf{u} \in \mathbb{R}^d$ , where  $\mathbf{Z} \sim \text{MGPD}(\mathbf{T}, \boldsymbol{\sigma}, \boldsymbol{\gamma})$ . Then, according to Proposition 2.1, the

---

<sup>2</sup>Degenerate cases can occur when  $p_1(v) = 0$ . For example, if  $\gamma^{(1)} < 0$ , the PN is not defined for  $v \geq u^{(1)} - \sigma^{(1)}/\gamma^{(1)}$ , which is visible for the dashed line in the left panel of Figure 3.

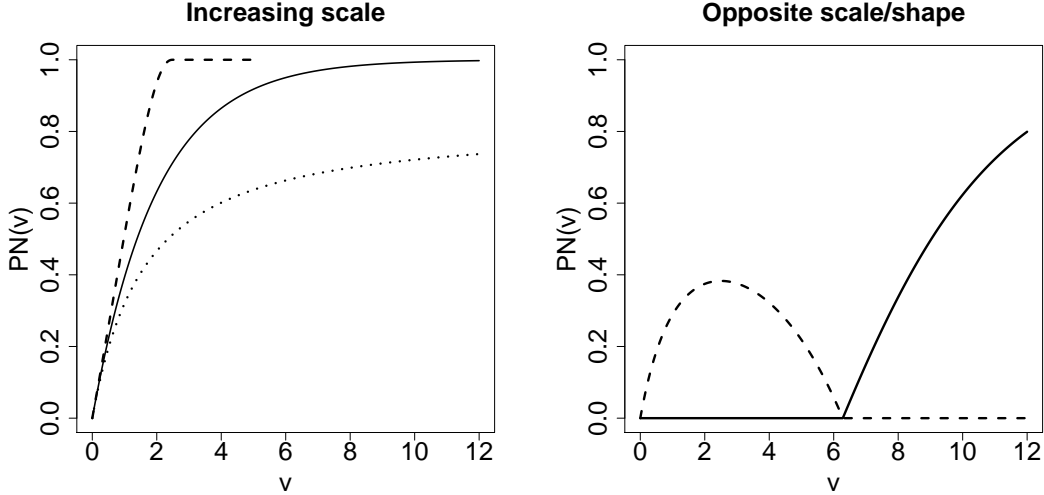


Figure 3: Probability of necessary causation as a function of  $v$ , see (2.3) and (3.1). Left panel: the counterfactual scale is  $\sigma^{(0)} = 1$ , increasing to  $\sigma^{(1)} = 2$  in the factual world, while the shape parameter is identical,  $\gamma^{(0)} = \gamma^{(1)}$ , equal to  $-0.4$ ,  $0$ , and  $0.4$  for the dashed, solid and dotted lines respectively. Right panel: the solid line corresponds to increasing shape and decreasing scale,  $(\gamma^{(0)}, \sigma^{(0)}) = (0, 2)$  and  $(\gamma^{(1)}, \sigma^{(1)}) = (0.4, 1)$ . The dashed line corresponds to the opposite scenario :  $(\gamma^{(0)}, \sigma^{(0)}) = (0.4, 1)$  and  $(\gamma^{(1)}, \sigma^{(1)}) = (0, 2)$ .

extremal information contained in any linear projection  $\mathbf{w}^T \mathbf{X}$  can be approximated, up to a normalizing constant, by a univariate GPD survival function. More precisely, for any  $v > \mathbf{w}^T \mathbf{u}$ , we can write

$$\mathbb{P}[\mathbf{w}^T \mathbf{X} > v] \approx \mathbb{P}[\mathbf{w}^T \mathbf{X} > \mathbf{w}^T \mathbf{u}] \bar{H}(v - \mathbf{w}^T \mathbf{u}; \mathbf{w}^T \boldsymbol{\sigma}, \gamma), \quad (4.1)$$

for  $w_1 + \dots + w_d = 1$  and  $\boldsymbol{\gamma} = \gamma \mathbf{1}_d$ . Constraining the weights to sum to a constant is necessary to ensure identification of  $\boldsymbol{\sigma}$ . The condition  $\boldsymbol{\gamma} = \gamma \mathbf{1}_d$  implies that conditional marginal distributions  $[Z_j \mid Z_j > 0]$  have equal shape parameters for  $j = 1, \dots, d$ . There-

fore, homogeneous spatial regions (in terms of the shape parameter) have to be identified in practice. This is closely related to the regional frequency analysis problem treated in hydrology (Carreau et al. 2017). Finally, we note that the dependence structure of  $\mathbf{X}$  is present in the term  $\mathbb{P}[\mathbf{w}^T \mathbf{X} > \mathbf{w}^T \mathbf{u}]$  only.

Any linear projection in the factual and counterfactuals worlds, denoted  $p_1(v; \mathbf{w}) = \mathbb{P}[\mathbf{w}^T \mathbf{X}^{(1)} > v]$  and  $p_0(v; \mathbf{w}) = \mathbb{P}[\mathbf{w}^T \mathbf{X}^{(0)} > v]$  respectively, can now be used to compute a probability of necessary causation that depends on the weight  $\mathbf{w}$  and the dependence structure of  $\mathbf{X}^{(0)}$  and  $\mathbf{X}^{(1)}$ ;

$$\text{PN}(v, \mathbf{w}) = \max \left( 1 - \frac{\mathbb{P}[\mathbf{w}^T \mathbf{X}^{(0)} > v]}{\mathbb{P}[\mathbf{w}^T \mathbf{X}^{(1)} > v]}, 0 \right), \quad (4.2)$$

where  $\mathbf{X}^{(i)}$  satisfies approximation (4.1) for  $i \in \{0, 1\}$ . To understand how dependence affects the strength of necessary causation, we study the value of  $\text{PN}(v, \mathbf{w})$  in the bivariate case with  $\mathbf{w} = (0.5, 0.5)$ ,  $\mathbf{X}^{(0)} \stackrel{d}{=} \mathbf{Z}^{(0)} \sim \text{MGPD}(\mathbf{T}^{(0)}, \boldsymbol{\sigma}^{(0)}, \mathbf{0})$  and  $\mathbf{X}^{(1)} \stackrel{d}{=} \mathbf{Z}^{(1)} \sim \text{MGPD}(\mathbf{T}^{(1)}, \boldsymbol{\sigma}^{(1)}, \mathbf{0})$ . In the example displayed in Figure 4, two different dependence structures are investigated, summarized by the tail dependence coefficient  $\chi$ . The dotted line corresponds to increasing dependence, from  $\chi^{(0)} = 0.3$  to  $\chi^{(1)} = 0.5$  and an increasing marginal scale, from  $\boldsymbol{\sigma}^{(0)} = (1, 1)$  to  $\boldsymbol{\sigma}^{(1)} = (2, 2)$ . The dashed line again represents increasing dependence, but decreasing marginal scale, from  $\boldsymbol{\sigma}^{(0)} = (2, 2)$  to  $\boldsymbol{\sigma}^{(1)} = (1, 1)$ . Finally, the solid line shows increasing marginal scale of the same order as the dotted line, and decreasing dependence, from  $\chi^{(0)} = 0.5$  to  $\chi^{(1)} = 0.3$ . Figure 4 shows that the dependence structure can have an impact on the PN for any finite value of  $v$ . In other words, EEA based on a hypothesis of independence (eg, in space) will lead to incomplete statements concerning the strength of PN whenever the multivariate extremes are dependent. Figure 4 also suggests that, as  $v$  increases, the impact of an increasing dependence in the factual world becomes negligible. However, it is important to keep in mind that in applications,

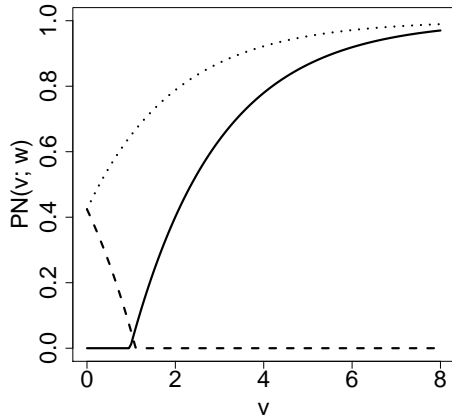


Figure 4:  $\text{PN}(v, \mathbf{w} = (0.5, 0.5))$  defined by (4.2) between two bivariate GPDs,  $\mathbf{Z}^{(0)} \sim \text{MGPD}(\mathbf{T}^{(0)}, \boldsymbol{\sigma}^{(0)}, \mathbf{0})$  and  $\mathbf{Z}^{(1)} \sim \text{MGPD}(\mathbf{T}^{(1)}, \boldsymbol{\sigma}^{(1)}, \mathbf{0})$ . The dotted line corresponds to  $\chi^{(0)} = 0.3$ ,  $\chi^{(1)} = 0.5$ ,  $\boldsymbol{\sigma}^{(0)} = (1, 1)$  and  $\boldsymbol{\sigma}^{(1)} = (2, 2)$ . The dashed line differs from the dotted line by  $\boldsymbol{\sigma}^{(0)} = (2, 2)$  and  $\boldsymbol{\sigma}^{(1)} = (1, 1)$ . The solid line differs from the dotted line by  $\chi^{(0)} = 0.5$  and  $\chi^{(1)} = 0.3$ .

the marginal scale might be constant between the two worlds. In that case, we will see the impact of increasing dependence in Figure 6.

## 4.2 Maximizing necessary causation

In a Gaussian set-up, Hannart & Naveau (2018) explored how to maximize causation probabilities of any Gaussian linear projection. Similarly here, the choice of  $\mathbf{w}$  could be an essential part in the maximization of necessary causation for multivariate GPD random variables. To address this point in the bivariate case, we need the following result.

**Proposition 4.1.** *Let  $\gamma \in \mathbb{R}$  and consider two positive bivariate scale parameters:*

$\boldsymbol{\sigma}^{(0)} = (\sigma_1^{(0)}, \sigma_2^{(0)})^T$  and  $\boldsymbol{\sigma}^{(1)} = (\sigma_1^{(1)}, \sigma_2^{(1)})^T$ . Denote

$$R = \frac{\left(\sigma_1^{(0)}\sigma_2^{(1)} - \sigma_2^{(0)}\sigma_1^{(1)}\right)\left(\sigma_1^{(0)}\sigma_2^{(1)} - \sigma_2^{(0)}\sigma_1^{(1)} + \gamma v \left\{(\sigma_2^{(1)} - \sigma_1^{(1)}) - (\sigma_2^{(0)} - \sigma_1^{(0)})\right\}\right)}{(\sigma_2^{(1)} - \sigma_1^{(1)})(\sigma_2^{(0)} - \sigma_1^{(0)}) \left\{(\sigma_2^{(1)} - \sigma_1^{(1)}) - (\sigma_2^{(0)} - \sigma_1^{(0)})\right\}^2},$$

and if  $R > 0$ , define the weights

$$w_{\pm}(v) = \frac{\sigma_2^{(1)} - \sigma_2^{(0)}}{(\sigma_2^{(1)} - \sigma_1^{(1)}) - (\sigma_2^{(0)} - \sigma_1^{(0)})} \pm \sqrt{R}.$$

If  $R \geq 0$  and if one of the two weights  $w_{\pm}(v)$  belongs to  $(0, 1)$ , then this weight, denoted  $w_{\text{opt}}$ , maximizes

$$\left\{ 1 - \frac{\bar{H}\left(v; w\sigma_1^{(0)} + (1-w)\sigma_2^{(0)}, \gamma\right)}{\bar{H}\left(v; w\sigma_1^{(1)} + (1-w)\sigma_2^{(1)}, \gamma\right)} \right\}. \quad (4.3)$$

In all other cases, only zero or unit weights maximize this ratio.

When  $\gamma = 0$ , the expression of  $w_{\pm}(v)$  is simpler because it does not depend on  $v$ . Expression (4.3) is an approximation of the PN defined in (4.2); it is equal to the PN when  $\mathbf{X}^{(0)}, \mathbf{X}^{(1)}$  are multivariate GPDs and  $\mathbb{P}[\mathbf{w}^T \mathbf{Z}^{(0)} > 0] = \mathbb{P}[\mathbf{w}^T \mathbf{Z}^{(1)} > 0]$ , i.e., when the dependence structure remains constant between the two worlds. Proposition 4.1 allows us to study the gain in terms of PN with respect to the weight  $w$ . When unit or zero weights are chosen as the optimal solution in Proposition 4.1, only one coordinate is considered and no linear projection is necessary. This happens when the contrast in one of the margins between the factual and counterfactual world is already sufficient to optimize PN. However, Proposition 4.1 shows that, to maximize necessary causality, one needs to consider only those components that (individually) give the largest PN. As an example, take  $\mathbf{X}^{(0)} \stackrel{d}{=} \mathbf{Z}^{(0)} \sim \text{MGPD}(\mathbf{T}^{(0)}, (1, 2)^T, \gamma \mathbf{1}_d)$  and  $\mathbf{X}^{(1)} \stackrel{d}{=} \mathbf{Z}^{(1)} \sim \text{MGPD}(\mathbf{T}^{(1)}, (1.5, 2)^T, \gamma \mathbf{1}_d)$ . The dependence structures of  $\mathbf{T}^{(1)}$  and  $\mathbf{T}^{(0)}$  are chosen such that  $\chi^{(0)} = \chi^{(1)} = 0.5$ . Hence, the

difference between the two worlds is only due to the scale change in one of the components. Figure 5 shows the PN gain as a function of  $v$ , i.e., the ratio between  $\text{PN}(v, (0.5, 0.5)^T)$  and  $\text{PN}(v, (w_{\text{opt}}, 1 - w_{\text{opt}})^T)$  where  $w_{\text{opt}} = 1$  based on Proposition 4.1. Each curve corresponds to a different shape parameter (with constraint  $\gamma^{(0)} = \gamma^{(1)}$ ), equal to  $-0.4$  (dashed line),  $0$  (solid line), and  $0.4$  (dotted line), respectively. We see that the optimal weight can lead to a large increase in necessary causality, particularly when the shape parameter is positive (dotted line).

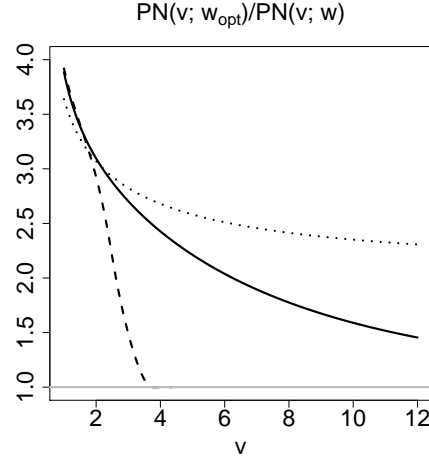


Figure 5: Necessary causation gain when  $\mathbf{X}^{(0)} \stackrel{d}{=} \mathbf{Z}^{(0)} \sim \text{MGPD}(\mathbf{T}^{(0)}, (1, 2)^T, \gamma \mathbf{1}_d)$  and  $\mathbf{X}^{(1)} \stackrel{d}{=} \mathbf{Z}^{(1)} \sim \text{MGPD}(\mathbf{T}^{(1)}, (1.5, 2)^T, \gamma \mathbf{1}_d)$ , and  $\mathbf{T}^{(1)}, \mathbf{T}^{(0)}$  are Gaussian random vectors with  $\chi^{(0)} = \chi^{(1)} = 0.5$ . The ratio of  $\text{PN}(v, (w_{\text{opt}}, 1 - w_{\text{opt}})^T)$  to  $\text{PN}(v, (0.5, 0.5)^T)$  is shown as a function of  $v$ , where  $w_{\text{opt}} = 1$  based on Proposition 4.1. The dashed, solid and dotted lines correspond to a shape parameter (with constraint  $\gamma^{(0)} = \gamma^{(1)}$ ) of  $-0.4$ ,  $0$  and  $0.4$  respectively.

Explicit optimal weights like in Proposition 4.1 can only be obtained in very specific cases. For example, for the bivariate Gaussian GPD with  $\gamma = 1$ , the probability  $\mathbb{P}[\mathbf{w}^T \mathbf{Z}^{(i)} >$

0] does not depend on  $\mathbf{w}$  (see Proposition A.1 in the Appendix). For most other cases, numerical optimization schemes have to be used, especially beyond the bivariate set-up. In order to move closer to practical applications, we need to couple this optimization procedure with inference in a multivariate context.

### 4.3 Inference

Let  $\mathbf{X}_1^{(0)}, \dots, \mathbf{X}_n^{(0)}$  and  $\mathbf{X}_1^{(1)}, \dots, \mathbf{X}_n^{(1)}$  denote two independent samples of size  $n$ , representing climate model output in the counterfactual and the factual world respectively, and let  $\mathbf{u}^{(0)}, \mathbf{u}^{(1)}$  denote two high thresholds. For  $i \in \{0, 1\}$ , let  $N_i$  denote the number of observations among  $\mathbf{X}_1^{(i)}, \dots, \mathbf{X}_n^{(i)}$  that have at least one component exceeding  $\mathbf{u}^{(i)}$ . Extracting these observations and subtracting  $\mathbf{u}^{(i)}$ , we obtain the multivariate GPD samples  $\mathbf{Z}_1^{(i)}, \dots, \mathbf{Z}_{N_i}^{(i)}$ . For  $v > \mathbf{w}^T \mathbf{u}^{(i)}$ , an estimator of  $p_i(v; \mathbf{w}) = \mathbb{P}[\mathbf{w}^T \mathbf{X}^{(i)} > v]$  and hence of the PN follows from approximation (4.1). The first term,  $\mathbb{P}[\mathbf{w}^T \mathbf{X}^{(i)} > \mathbf{w}^T \mathbf{u}^{(i)}]$ , can be estimated nonparametrically by

$$\hat{p}_i^{(\text{emp})}(v; \mathbf{w}) = \frac{1}{n} \sum_{t=1}^n \mathbb{1} \left\{ \mathbf{w}^T \mathbf{X}_t^{(i)} > v \right\}.$$

To estimate the second term,  $\bar{H}(v - \mathbf{w}^T \mathbf{u}^{(i)}; \mathbf{w}^T \boldsymbol{\sigma}^{(i)}, \gamma^{(i)})$ , we first compute estimators  $\hat{\boldsymbol{\sigma}}^{(i)}$  and  $\hat{\gamma}^{(i)}$  by applying the method of probability weighted moments to  $(Z_{tj}^{(i)} \mid Z_{tj}^{(i)} > 0)_{t=1, \dots, N_i}$  for  $j \in \{1, \dots, d\}$  (see Appendix B). Next, we set  $\hat{\gamma}^{(i)} = d^{-1} \sum_{j=1}^d \hat{\gamma}_j^{(i)}$ <sup>3</sup>. Finally, we estimate  $p_i(v; \mathbf{w})$  by

$$\hat{p}_i(v; \mathbf{w}) = \begin{cases} \hat{p}_i^{(\text{emp})}(v; \mathbf{w}) & \text{if } v \leq \mathbf{w}^T \mathbf{u}^{(i)}, \\ \hat{p}_i^{(\text{emp})}(\mathbf{w}^T \mathbf{u}^{(i)}; \mathbf{w}) \bar{H}(v - \mathbf{w}^T \mathbf{u}^{(i)}; \mathbf{w}^T \hat{\boldsymbol{\sigma}}^{(i)}, \hat{\gamma}^{(i)}) & \text{if } v \leq \mathbf{w}^T \mathbf{u}^{(i)}. \end{cases} \quad (4.4)$$

---

<sup>3</sup>An alternative method to enforce equal shape parameters is described in Carreau et al. (2017)

Alternatively, we could directly estimate  $\gamma^{(i)}$  and  $\mathbf{w}^T \boldsymbol{\sigma}^{(i)}$  by applying the method of probability weighted moments to  $(\mathbf{w}^T \mathbf{Z}_t^{(i)} \mid \mathbf{w}^T \mathbf{Z}_t^{(i)} > 0)_{t=1,\dots,N_i}$ , which reduces uncertainty and enforces the constraint of equal shape parameters. Appendix C shows a small simulation experiment, confirming the good performance of  $\widehat{\text{PN}} = 1 - \widehat{p}_0/\widehat{p}_1$ .

In the previous sections, we studied the increase in PN for changing dependence structures and marginal parameters. Another important question is what happens when marginal parameters do not change ( $\boldsymbol{\sigma}^{(0)} = \boldsymbol{\sigma}^{(1)}$  and  $\boldsymbol{\gamma}^{(0)} = \boldsymbol{\gamma}^{(1)}$ ), while dependence increases ( $\chi^{(1)} > \chi^{(0)}$ ). Under a hypothesis of independence in space, one would estimate the univariate PN componentwise and take the average, thus possibly underestimating the PN. To see by how much, and how the result varies with the dimension, we conduct the following experiment. Consider  $d = 9$  points on a regular  $3 \times 3$  unit distance grid. For distances from 1 to  $\sqrt{8}$ , pairwise tail dependence coefficients ranging from 0.4 to 0.3 for the counterfactual world and from 0.55 to 0.4 for the factual world were obtained using a Whittle-Matérn correlation function<sup>4</sup>. We evaluate the PN in the 99% quantile of  $\mathbf{w}^T \mathbf{Z}^{(0)}$  using equal weights, calculated based on a pre-simulation run of sample size  $10^6$  and held fixed. Figure 6 shows boxplots of the multivariate estimates  $\widehat{\text{PN}}$  minus the average univariate PN estimates, based on 1000 samples of size  $n = 2000$ . The black line corresponds to the true values, calculated using the formulas in Appendix A. We see that as the dimension increases, taking dependence into account increases necessary causation.

---

<sup>4</sup>The covariance matrices  $\Sigma^{(0)}$  and  $\Sigma^{(1)}$  are generated using a Whittle-Matérn correlation function with fixed shape  $\kappa^{(0)} = \kappa^{(1)} = 1$  and varying scales  $\phi^{(0)} = 1$ ,  $\phi^{(1)} = 2.5$ . The correlation matrices are then multiplied by 10 to obtain  $\Sigma^{(0)}$  and  $\Sigma^{(1)}$

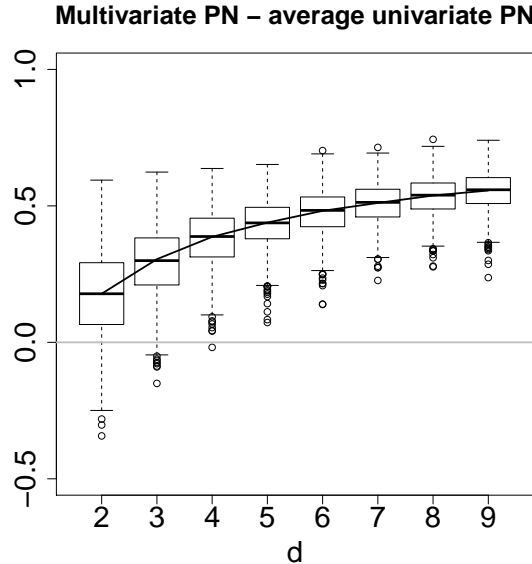


Figure 6: Boxplots of the multivariate estimates  $\widehat{PN} = 1 - \widehat{p}_0/\widehat{p}_1$  minus the average univariate PN estimates, where  $\widehat{p}_i$  is defined in (4.4), and  $d \in \{2, \dots, 9\}$ . 1000 samples of size  $n = 2000$  were simulated from a multivariate Gaussian GPD model with  $\boldsymbol{\sigma}^{(0)} = \boldsymbol{\sigma}^{(1)} = 1$  and  $\boldsymbol{\gamma}^{(0)} = \boldsymbol{\gamma}^{(1)} = 0$ ,  $\chi^{(0)} \in [0.3, 0.4]$  and  $\chi^{(1)} \in [0.4, 0.55]$  (pairwise). The black line corresponds to the true values.

## 5 Analysis of heavy precipitation from the CNRM model

Evidencing causality is more difficult for heavy rainfall than for extreme temperatures, because precipitation variability is greater in space and time and because extreme rainfall has heavier tails than temperatures (extreme rainfall often has  $\gamma \approx 0.2$ , see, e.g. Katz et al. (2002)). We want to determine if a multivariate GPD approach could enhance the

causality message of a univariate analysis. We work with simulated rainfall time series from the French global climate model of Météo-France (CNRM) that belongs to the latest Coupled Model Intercomparison Project (CMIP6). We consider the winter months between the 1st of January 1985 until the 31st of August 2014 over the region defined by  $-10$  to  $40$  in longitude and  $35$  to  $60$  in latitude (corresponding to central Europe). Our factual and counterfactual worlds correspond to two historical runs, the second one of which has only natural forcings. We take the weekly maxima of winter precipitation. As the number of years covers only three decades, the rainfall series can be considered stationary in time within each world. Concerning their spatial structure, we apply the partitioning around medoids (PAM) algorithm (Kaufman & Rousseeuw 1990) to the counterfactual rainfall run. The difference with the original PAM version is that our “distance” between two locations  $s$  and  $t$  is tailored to threshold exceedances via

$$\hat{d}_{st} = \frac{1 - \hat{\chi}_{st}}{2(3 - \hat{\chi}_{st})},$$

where  $\hat{\chi}_{st}$  denotes the standard empirical estimator of the pairwise tail dependence coefficient (see, e.g. Kiriliouk et al. 2016, and references therein). Our approach is close to the one of Bernard et al. (2013), who focused on maxima instead of threshold exceedances. Figure 7 displays the spatial structure for  $K = 40$  clusters<sup>5</sup>. Although no spatial coordinates were given to the algorithm, the clusters appear to be spatially homogeneous and climatologically coherent. As the multivariate GPD is tailored for asymptotic dependence, identifying dependent regions help improve its fit. In addition, such a spatial clustering makes the assumption of a constant shape parameter within a region more reasonable. We hence model each cluster independently, calculating the estimated multivariate PN based on  $\hat{p}_0, \hat{p}_1$  defined in (4.4). Figures 8 and 9 show necessity causation probabilities for the

---

<sup>5</sup>Other values of  $K$  were tested and provided similar patterns.

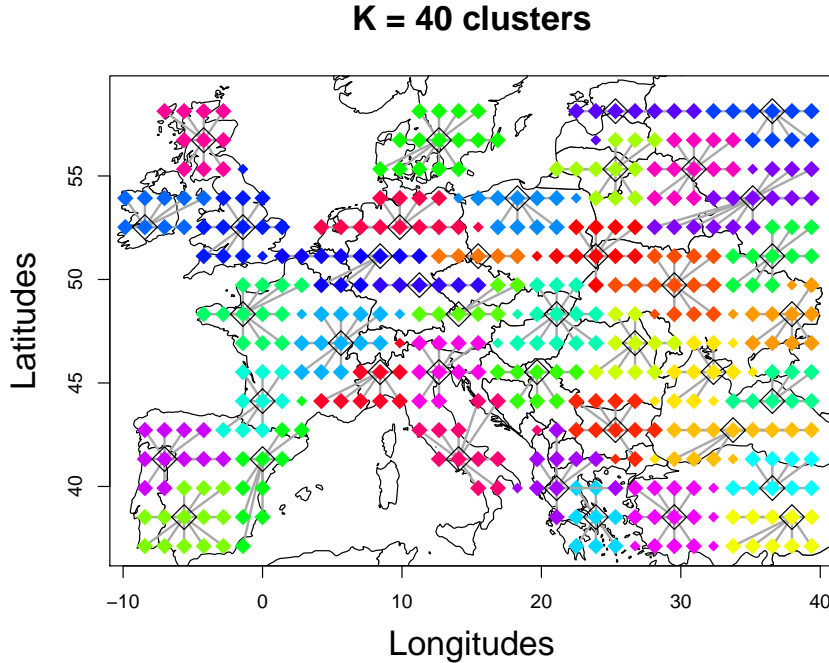


Figure 7: Clustering of weekly maximum winter precipitation in central Europe between January 1985 and August 2014, using the PAM algorithm with distance based on pairwise tail dependence coefficients.

five-year and fifty-year return level respectively. The return levels were calculated based on quantiles of  $\mathbf{w}^T \mathbf{X}^{(0)}$  for each cluster, with equal weights. Both figures show the PN per cluster, calculated using equal weights (top) and optimal weights (bottom). The diameters of the black circles around the PN estimates are proportional to the length of bootstrap-based 95% confidence intervals.

Higher PN does not necessarily come with higher uncertainty; see for instance the cluster around northern Italy, whose confidence interval is narrow for the five-year return level and even more so for the fifty-year return level. Comparing the two panels of Figure

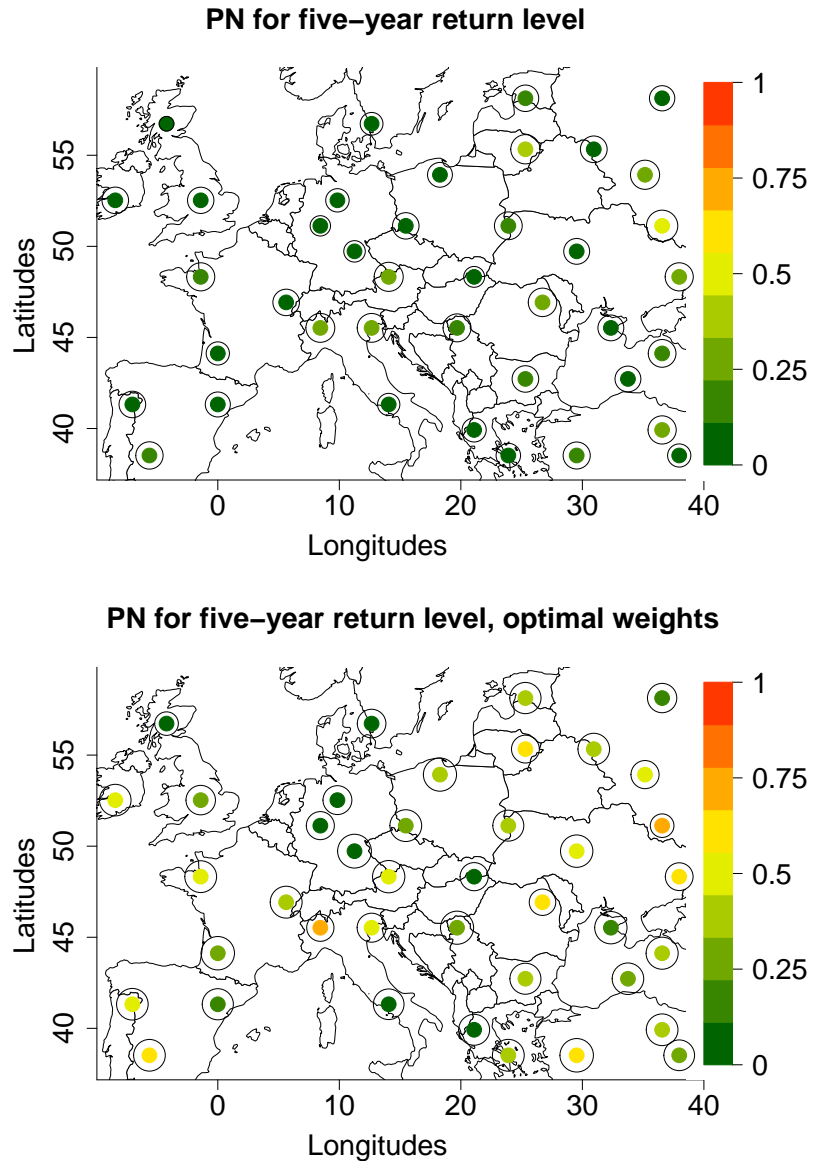


Figure 8: Necessary causation probabilities for a five-year return level of weighted maximal weekly winter precipitation in the counterfactual world for each cluster, calculated using equal weights (top) and optimal weights (bottom).

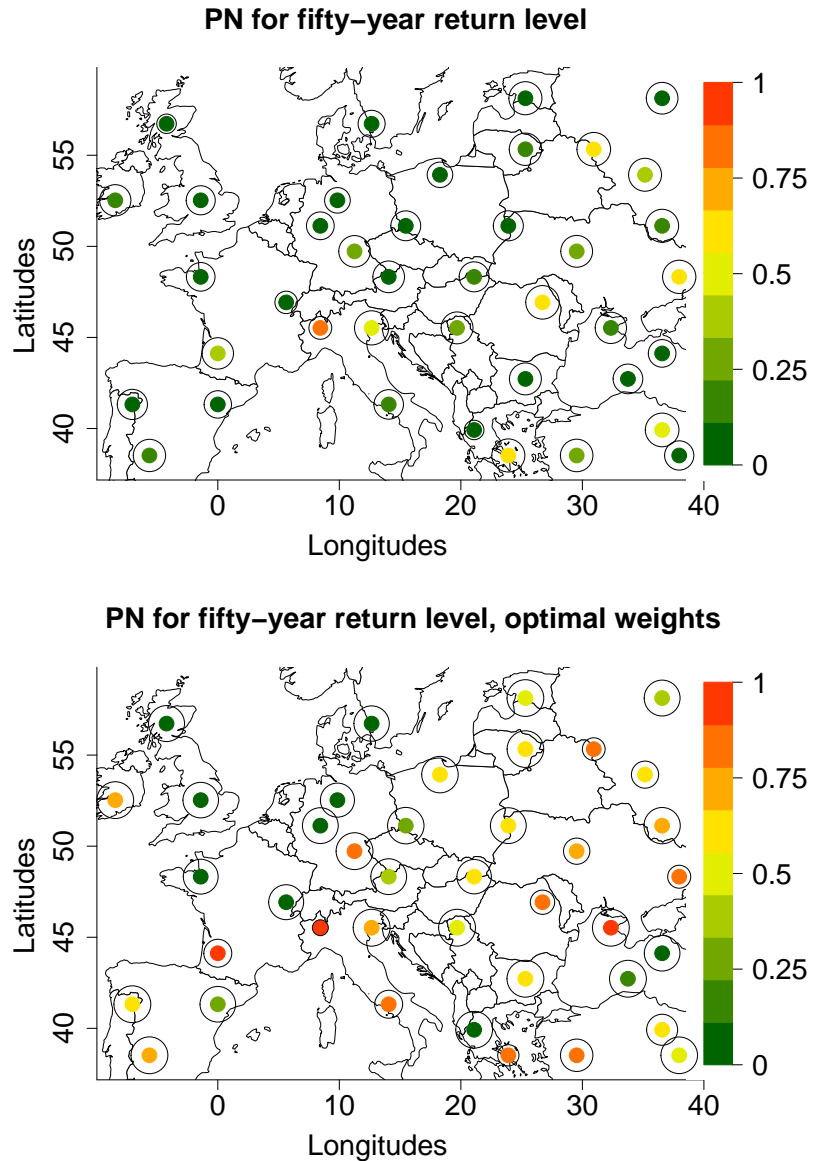


Figure 9: Necessary causation probabilities for a fifty-year return level of weighted maximal weekly winter precipitation in the counterfactual world for each cluster, calculated using equal weights (top) and optimal weights (bottom).

8 shows that the differences between the factual and the counterfactual world are higher when using optimal weights. This feature is even more striking for the fifty-year return levels, see Figure 9. Except for locations near the English channel, most points have a probability of necessary causation that is greater than 0.5. In particular, a few points like northern Italy shows a probability near one.

This example based on CRNM precipitation data is not sufficient to conclude general climatological results about heavy rainfall. The patterns found here may be due to this specific climate model, internal climate variability or other sources of variability. An exhaustive analysis of all the CMIP6 models, in terms of computer resources and climatological expertise, is beyond the scope of this methodological work. Still, this example illustrates that methods combining multivariate extreme-value theory and counterfactual theory could help climatologists working on causality and multivariate extremes (see, e.g. Kim et al. 2016, Zscheischler et al. 2018). Another interesting research direction will be to extend this coupling between EVT and counterfactual theory to other types of extremes modelling in geosciences; see, e.g. Hammerling et al. (2017) or Reich et al. (2013) for a Bayesian hierarchical point of view, Shooter et al. (2019) for asymptotic independence models, and Ragone et al. (2018) for rare event algorithms.

## A Gaussian multivariate GPD model

Let  $\mathbf{Z} \sim \text{MGPD}(\mathbf{T}, \boldsymbol{\sigma}, \boldsymbol{\gamma})$  and let  $\mathbf{T}$  be a bivariate Gaussian random vector with mean  $\mathbf{0}$  and covariance matrix  $\Sigma = (s_{tj})_{t,j=1,2}$ . Note that  $T_1 - T_2 \sim \mathcal{N}(0, \tau^2)$  with  $\tau^2 = s_{11} + s_{22} - 2s_{12}$ . The tail dependence coefficient defined in Section 2.1 can be shown to equal

$$\chi = 2 \left( 1 - \frac{1}{1 + 2e^{\tau^2/2}\Phi(-\tau)} \right),$$

see the supplementary material in Kiriliouk et al. (2019). In particular,  $\chi \rightarrow 0$  as  $\tau \rightarrow \infty$ . Since  $\chi$  is identified from  $\tau$ , different covariance matrices  $\Sigma$  may lead to the same tail dependence coefficient.

The Gaussian GPD model is convenient because the probability  $\mathbb{P}[\mathbf{w}^T \mathbf{Z} > 0]$ , which appears in the definition of the PN, can be calculated analytically in certain cases.

**Proposition A.1.** *Let  $\mathbf{Z} \sim \text{MGPD}(\mathbf{T}, \boldsymbol{\sigma}, (\gamma, \gamma))$  where  $\mathbf{T}$  is a bivariate Gaussian random vector with mean zero and covariance matrix  $\Sigma = (s_{tj})_{t,l=1,2}$ . Let  $\tau^2 = s_{11} + s_{22} - 2s_{12}$ .*

1. *If  $\gamma = 0$ , then for  $\delta := w_1 \sigma_1(\mathbf{w}^T \boldsymbol{\sigma})^{-1}$ , we have*

$$\mathbb{P}[\mathbf{w}^T \mathbf{Z} > 0] = e^{-\tau^2(\delta-1)^2} \Phi(\tau(\delta-1)) + e^{-\tau^2\delta^2} \Phi(-\tau\delta).$$

2. *If  $\gamma = 1$ , then*

$$\mathbb{P}[\mathbf{w}^T \mathbf{Z} > 0] = e^{\tau^2/2} \Phi(-\tau) + \frac{1}{2}.$$

For  $\gamma = 1$ , the probability  $\mathbb{P}[\mathbf{w}^T \mathbf{Z} > 0]$  does not depend on  $\mathbf{w}$ . This is no longer true when  $d > 2$ . For a generalization of Proposition A.1 and its proof, see the supplementary material.

## B Probability weighted moments inference

In this paper we opt for the probability weighted moments method of Hosking & Wallis (1987) to estimate the parameters of a univariate GPD, because of its simplicity and its popularity in hydrological sciences. The method performs well for<sup>6</sup>  $\gamma < 1/2$ , and the asymptotic covariance matrix has a simple expression (Hosking & Wallis 1987, Ribereau

---

<sup>6</sup>An extension has been proposed for  $\gamma < 1$  (Diebolt et al. 2007).

et al. 2011). Let  $Z_1, \dots, Z_N$  denote iid copies of  $Z \sim \text{GPD}(\sigma, \gamma)$ . The first and second probability weighted moments of  $Z$  are

$$\mu = \mathbb{E}[Z] = \frac{\sigma}{(1 - \gamma)}, \quad \beta = \mathbb{E}[Z \bar{H}(Z; \sigma, \gamma)] = \frac{\sigma}{2(3 - \gamma)}.$$

These probability weighted moments can be estimated by

$$\hat{\mu} = \frac{1}{N} \sum_{i=1}^N Z_i, \quad \hat{\beta} = \frac{1}{N} \sum_{i=1}^N \frac{(N-i)}{(N-1)} Z_{(i)},$$

where  $Z_{(1)} < \dots < Z_{(N)}$  are the order statistics of  $Z_1, \dots, Z_N$ , which gives

$$\hat{\sigma} = \frac{2\hat{\mu}\hat{\beta}}{\hat{\mu} - 2\hat{\beta}}, \quad \hat{\gamma} = 2 - \frac{\hat{\mu}}{\hat{\mu} - 2\hat{\beta}}.$$

## C Simulation

Let  $\mathbf{Z}^{(i)} \sim \text{MGPD}(\mathbf{T}^{(i)}, \boldsymbol{\sigma}^{(i)}, \mathbf{0}_d)$  and let  $\mathbf{T}^{(i)}$  follow a Gaussian distribution with mean zero and covariance matrix  $\Sigma^{(i)}$ . We assess the quality of the estimator  $\hat{p}_i$  in (4.4) for a range of thresholds  $v$ . The true probabilities  $p_i$  can be calculated by combining (4.1) with Proposition A.1 (or its  $d$ -dimensional generalization in the supplementary material). The experiments are based on 1000 samples of size  $n = 500$  from  $\mathbf{Z}^{(i)}$  with  $\mathbf{u}^{(i)} = \mathbf{0}$ . Figure 10 shows the results for  $d \in \{2, 4\}$  and  $v \in \{0, 1, \dots, 7\}$ , where  $v = 7$  roughly corresponds to the 99.9% quantile of  $\mathbf{w}^T \mathbf{Z}^{(0)}$ . We take  $\mathbf{w} = (1/d, \dots, 1/d)$ ; using the optimal weights gives similar results (not shown). We consider increasing dependence ( $\chi^{(0)} = 0.3$ ,  $\chi^{(1)} = 0.5$ ), increasing marginal scale ( $\boldsymbol{\sigma}^{(0)} = \mathbf{1}_d$ ,  $\boldsymbol{\sigma}^{(1)} = \mathbf{2}_d$ ) and constant marginal shape ( $\boldsymbol{\gamma}^{(0)} = \boldsymbol{\gamma}^{(1)} = \mathbf{0}_d$ ). Boxplots of the corresponding estimators of the PN are centered around their true values for better visibility. We see that the estimated median is always equal to the true one. As  $v$  increases, more and more (downward) outliers appears,

which is natural as the true PN is very close to 1 for large values of  $v$ . For small values of  $v$ , the results show less variability for  $d = 2$  than for  $d = 4$ , while for large  $v$ , the opposite happens.

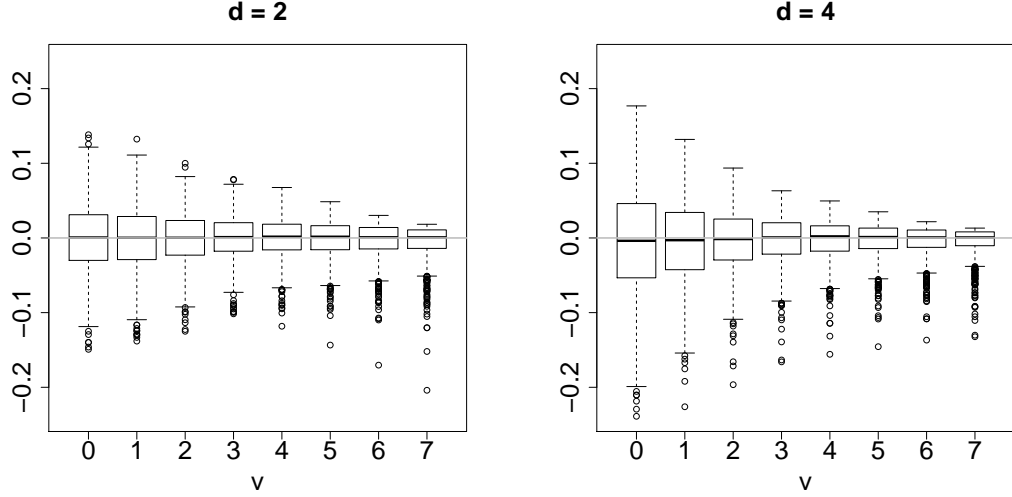


Figure 10: Boxplots of estimators of PN based on (4.4), centered around their true values, based on 1000 samples of size  $n = 500$  from  $\mathbf{Z}^{(i)}$  with  $\chi^{(0)} = 0.3$ ,  $\chi^{(1)} = 0.5$ ,  $\boldsymbol{\sigma}^{(0)} = \mathbf{1}_d$ ,  $\boldsymbol{\sigma}^{(1)} = \mathbf{2}_d$  and  $\boldsymbol{\gamma}^{(0)} = \boldsymbol{\gamma}^{(1)} = \mathbf{0}_d$ , for equal weights in  $d = 2$  (left panel) and  $d = 4$  (right panel).

## REFERENCES

Angélil, O., Stone, D. & Wehner, M. (2017), ‘An independent assessment of anthropogenic attribution statements for recent extreme temperature and rainfall events’, *Journal of Climate* **30**, 5–16.

Balkema, A. A. & de Haan, L. (1974), 'Residual life time at great age', *The Annals of Probability* **2**(5), 792–804.

Beirlant, J., Goegebeur, Y., Segers, J. & Teugels, J. (2004), *Statistics of Extremes: Theory and Applications*, Wiley.

Bernard, E., Naveau, P., Vrac, M. & Mestre, O. (2013), 'Clustering of maxima: Spatial dependencies among heavy rainfall in France', *Journal of Climate* **26**(20), 7929–7937.

Carreau, J., Naveau, P. & Neppel, L. (2017), 'Partitioning into hazard subregions for regional peaks-over-threshold modeling of heavy precipitation', *Water Resources Research* **53**(5), 4407–4426.

Chen, Y., Moufouma-Okia, W., Masson-Delmotte, V., Zhai, P. & Pirani, A. (2018), 'Recent progress and emerging topics on weather and climate extremes since the fifth assessment report of the intergovernmental panel on climate change', *Annual Review of Environment and Resources* **43**(1), 35–59.

Coles, S. G. (2001), *An Introduction to Statistical Modeling of Extreme Values*, Springer-Verlag Inc.

Cooley, D., Hunter, B. & Smith, R. L. (2017), *Handbook of Environmental and Ecological Statistics*, CRC Press, chapter Univariate and Multivariate Extremes for the Environmental Sciences.

Davison, A. C. & Smith, R. L. (1990), 'Models for exceedances over high thresholds (with comments)', *Journal of the Royal Statistical Society: Series B (Statistical Methodology)* **52**(3), 393–442.

Davison, A. & Huser, R. (2015), ‘Statistics of extremes’, *Annual Review of Statistics and Its Application* **2**(1), 203–235.

de Fondeville, R. & Davison, A. (2018), ‘High-dimensional peaks-over-threshold inference’, *Biometrika* **105**(3).

de Fondeville, R. & Davison, A. (2019), ‘Functional peaks-over-threshold analysis and generalized r-Pareto process’, *Preprint*.

Diebolt, J., Guillou, A. & Rached, I. (2007), ‘Approximation of the distribution of excesses through a generalized probability-weighted moments method’, *Journal of Statistical Planning and Inference* **137**(3), 841–857.

Embrechts, P., Klüppelberg, C. & Mikosch, T. (1997), *Modelling Extremal Events for Insurance and Finance*, Vol. 33, Applications of Mathematics, Springer-Verlag, Berlin.

Engelke, S., De Fondeville, R. & Oesting, M. (2018), ‘Extremal behaviour of aggregated data with an application to downscaling’, *Biometrika* **106**(1), 127–144.

Falk, M. & Guillou, A. (2008), ‘Peaks-over-threshold stability of multivariate generalized Pareto distributions’, *Journal of Multivariate Analysis* **99**(4), 715–734.

Ferreira, A. & de Haan, L. (2014), ‘The generalized Pareto process; with a view towards application and simulation’, *Bernoulli* **20**(4), 1717–1737.

Fischer, E. M. & Knutti, R. (2015), ‘Anthropogenic contribution to global occurrence of heavy-precipitation and high-temperature extremes’, *Nature Climate Change* **5**(6), 560–564.

Hammerling, D., Katzfuss, M. & Smith, R. L. (2017), *Handbook of Environmental and Ecological Statistics*, CRC Press, chapter Climate Change Detection and Attribution.

Hannart, A. & Naveau, P. (2018), ‘Probabilities of causation of climate changes’, *Journal of Climate* **31**(14), 5507–5524.

Hannart, A., Pearl, J., Otto, F., Naveau, P. & Ghil, M. (2016), ‘Causal counterfactual theory for the attribution of weather and climate-related events’, *Bulletin of the American Meteorological Society* **97**(1), 99–110.

Hosking, J. R. & Wallis, J. R. (1987), ‘Parameter and quantile estimation for the generalized Pareto distribution’, *Technometrics* **29**(3), 339–349.

Huser, R., Davison, A. C. & Genton, M. G. (2016), ‘Likelihood estimators for multivariate extremes’, *Extremes* **19**(1), 79–103.

Katz, R., Parlange, M. & Naveau, P. (2002), ‘Extremes in hydrology’, *Water Res.* **25**, 1287–1304.

Katzfuss, M., Hammerling, D. & Smith, R. L. (2017), ‘A Bayesian hierarchical model for climate change detection and attribution’, *Geophys. Res. Lett.* **11**(44), 5720–5728.

Kaufman, L. & Rousseeuw, P. J. (1990), *Finding groups in data: an introduction to cluster analysis*, Wiley Online Library.

Kew, S. f., Philip, S. Y., Jan van Oldenborgh, G., van der Schrier, G., Otto, F. E. L. & Vautard, R. (2019), ‘The exceptional summer heat wave in southern Europe 2017’, *Bulletin of the American Meteorological Society* **100**(1), S49–S53.

Kharin, V. V. & Zwiers, F. W. (2005), ‘Estimating extremes in transient climate change simulations.’, *Journal of Climate* **18**, 1156–1173.

Kharin, V. V., Zwiers, F. W., Zhang, X. & Hegerl, G. C. (2007), ‘Changes in temperature and precipitation extremes in the IPCC ensemble of global coupled model simulations’, *Journal of Climate* **20**(8), 1419–1444.

Kim, Y.-H., Min, S.-K., Zhang, X., Zwiers, F., Alexander, L. V., Donat, M. G. & Tung, Y.-S. (2016), ‘Attribution of extreme temperature changes during 1951–2010’, *Climate Dyn.* **46**, 1769–1782.

King, A. D. (2017), ‘Attributing changing rates of temperature record breaking to anthropogenic influences’, *Earth’s Future* **5**, 1156–1168.

Kiriliouk, A., Rootzén, H., Segers, J. & Wadsworth, J. L. (2019), ‘Peaks over thresholds modelling with multivariate generalized Pareto distributions’, *Technometrics* **61**(1), 123–135.

Kiriliouk, A., Segers, J. & Warchał, M. (2016), Nonparametric estimation of extremal dependence, in ‘Extreme Value Modeling and Risk Analysis: Methods and Applications’, CRC Press.

Luu, L. N., Vautard, R., Yiou, P., van Oldenborgh, G. J. & Lenderink, G. (2018), ‘Attribution of extreme rainfall events in the south of France using EURO-CORDEX simulations’, *Geophysical Research Letters* **45**, 6242–6250.

National Academies of Sciences, Engineering and Medicine (2016), *Attribution of Extreme Weather Events in the Context of Climate Change*, The National Academies Press, Washington, DC.

Otto, F. E., Philip, S., Kew, S., Li, S., King, A. & Cullen, H. (2018), ‘Attributing high-impact extreme events across timescalesa case study of four different types of events’, *Climatic change* **149**(3-4), 399–412.

Paciorek, C. J., Stone, D. A. & Wehner, M. F. (2018), ‘Quantifying statistical uncertainty in the attribution of human influence on severe weather’, *Weather and Climate Extremes* **20**, 69 – 80.

Pearl, J. (2000), *Causality: Models, reasoning, and inference.*, Cambridge University Press.

Pickands, J. (1975), ‘Statistical inference using extreme order statistics’, *The Annals of Statistics* **3**(1), 119–131.

Ragone, F., Wouters, J. & Bouchet, F. (2018), ‘Computation of extreme heat waves in climate models using a large deviation algorithm’, *Proceedings of the National Academy of Sciences* **115**(1), 24–29.

Reich, B., Shaby, B. & Cooley, D. (2013), ‘A hierarchical model for serially dependent extremes: a study of heat waves in the western US.’, *J. Agric. Biol. Environ. Stat.* **19**, 119–135.

Ribereau, P., Naveau, P. & Guillou, A. (2011), ‘A note of caution when interpreting parameters of the distribution of excesses’, *Advances in Water Resources* **34**(10), 1215–1221.

Rootzén, H., Segers, J. & Wadsworth, J. L. (2018a), ‘Multivariate generalized Pareto distributions: parametrizations, representations and properties’, *Journal of Multivariate Analysis* **165**(1), 117–131.

Rootzén, H., Segers, J. & Wadsworth, J. L. (2018b), ‘Multivariate peaks over thresholds models’, *Extremes* **21**(1), 115–145.

Rootzén, H. & Tajvidi, N. (2006), 'Multivariate generalized Pareto distributions', *Bernoulli* **12**(5), 917–930.

Shaby, B. & Reich, B. (2012), 'Bayesian spatial extreme value analysis to assess the changing risk of concurrent high temperatures across large portions of European cropland', *Environmetrics* **23**, 638–48.

Shooter, R., Ross, E., Tawn, J. & Jonathan, P. (2019), 'On spatial conditional extremes for ocean storm severity', *Environmetrics* **1**, 1–18.

Stott, P. A., Christidis, N., Otto, F. E. L., Sun, Y., Vanderlinden, J.-P., van Oldenborgh, G., R. Vautard, von Storch, H., Walton, P., Yiou, P. & Zwiers, F. W. (2016), 'Attribution of extreme weather and climate-related events', *WIREs Clim Change* **7**(23–41).

Stott, P. A., Stone, D. A. & Allen, M. R. (2004), 'Human contribution to the European heatwave of 2003', *Nature* **432**(7017), 610.

Tajvidi, N. (1996), Characterisation and Some Statistical Aspects of Univariate and Multivariate Generalized Pareto Distributions, PhD thesis, Department of Mathematics, Chalmers, Göteborg.

Zscheischler, J., Westra, S., van den Hurk, B. J. J. M., Seneviratne, S. I., Ward, P. J., Pitman, A., AghaKouchak, A., Bresch, D. N., Leonard, M., Wahl, T. & Zhang, X. (2018), 'Future climate risk from compound events', *Nature Climate Change* **8**(6), 469–477.